ORIGINAL PAPER

Solvatochromic Studies of Fluorescent Azo Dyes: Kamlet-Taft (π*, α and β) and Catalan (S$_{pp}$, S$_A$ and S$_B$) Solvent Scales Approach

Jayaraman Jayabharathi · Venugopal Thanikachalam · Marimuthu Venkatesh Perumal · Karunamoorthy Jayamoorthy

Abstract A new metal ion-responsive azo-based fluorescent probes have been synthesized and characterized by NMR spectral techniques. Steady-state fluorometric study has been used to analyze the spectroscopic and photophysical characteristics of dye derivatives in various solvents. The fluorescence properties of these dyes are strongly solvent dependent, the wavelength of maximum fluorescence emission shifts to the red. The Kamlet-Taft and Catalan's solvent scales were found to be the most suitable for describing the solvatochromic shifts of the absorption and fluorescence emission. The hydroxy substituted azo dye formed complexes with several metal ions (Co^{2+}, Hg^{2+}, Ni^{2+} and Cu^{2+}) and fluorescence quenching with metal ions reveal that it can be used as a new fluorescence sensor to detect the Cu^{2+} ion.

Introduction

Measurements of concentration of analytically and biologically important ions by fluorescent chemosensors are indispensable tool in numerous fields of modern medicine and science. The design and development of fluorescent probes for metal ion analysis remains an active research field. Azo compounds are versatile molecules, forming stable complexes with metal ions and have received much attention in research

in the view of both fundamental and applications [1–5]. Though atomic emission or mass spectroscopy (ICP-AES, ICP-MS) used to detect heavy metals at low concentrations, they are very expensive, therefore fluorescence sensors have been developed [6–10]. Copper exists in human body, plants and animals in trace amounts; however, high amount can cause serious health problems such as nausea, vomiting and diarrhea as well as damage to liver and kidneys [11]. Therefore, in the view of the biological and environmental importance, considerable attention has been focused on detection of Cu(II) ion [12, 13] by quenching of fluorescence intensity of the employed sensing material [14–17].

Several factors contribute to the best laser performance of dyes namely, low triplet-triplet absorption capacity, a poor tendency to self-aggregate in organic solvents and their high photo stability, which improves the lifetime of the laser action [11–17]. The Stokes shift modifies the lasing performance [18] in highly concentrated solutions because it affects the reabsorption and reemission phenomena, which shifts the emission band to longer wavelength and reduces its efficiency. In the present paper, we exploited the photophysical characterization of dye derivatives **1**–**4** in various solvents and the solvent effects were analyzed using two different solvent scales namely Kamlet-Taft (π*, α and β) and Catalan parameters (Spp, SA and SB) (multicomponent linear regression).

Experimental

Materials and Methods

Aniline (Sigma-Aldrich Ltd.), Furan-2-carboxaldehyde, Thiophene-2-carboxaldehyde, Pyridine-2-caroboxaldehyde,

J. Jayabharathi (✉) · V. Thanikachalam · M. V. Perumal · K. Jayamoorthy
Department of Chemistry, Annamalai University, Annamalainagar 608 002 Tamilnadu, India
e-mail: jtchalam2005@yahoo.co.in

Table 1 Photoluminescence spectral data of various solvents and solid emission spectra of picrate derivatives **1–4**

Solvent	Absorption[a] (λ, nm)				Emission[b] (λ, nm)				Stokes shift (cm^{-1})			
	1	2	3	4	1	2	3	4	1	2	3	4
n-Hexane	362	357	360	371	402	407	419	413	2749	3441	3911	2741
1,4-dioxane	368	365	368	372	415	417	423	413	3078	3416	3533	2669
Benzene	364	360	365	371	412	414	421	423, 480	3201	3623	3644	3314
Chloroform	369	368	367	375	423	426	428	414	3460	3700	3883	2512
Ethyl acetate	370	369	371	385	427	429	430	427	3608	3790	3698	2555
Dichloromethane	372 (375)[c]	374 (380)[c]	373 (379)[c]	376 (381)[c]	428	434	432	418	3517	3696	3662	2672
Butanol	370	377	378	361, 401	427	435	434	441	3608	3537	3414	2262
Ethanol	374	381	383	392, 420	428	437	436	440	3373	3363	3174	1082
Methanol	375	383	384	370, 400	432	436	437	439	3519	3174	3158	2221
Acetonitrile	379	387	388	375	434	438	440	424	3344	3009	3046	3039

[a] UV-vis absorption measured in solution concentration = 1×10^{-5} M

[b] Photoluminescence measured in solution concentration = 1×10^{-4} M

[c] λ_{abs} calculated by Gaussion-03

3-hydroxypyridin-2-carboxaldehyde, (S.D. fine.) and all other Reagents were used without further purification.

Optical Measurements and Computational Details

NMR spectra were recorded on a Bruker 400 MHz The ultraviolet–visible (UV–vis) spectra were measured on

UV–vis spectrophotometer (Perkin Elmer, Lambda 35) and corrected for background due to solvent absorption. Photoluminescence (PL) spectra were recorded on a (Perkin Elmer LS55) fluorescence spectrometer. MS spectra were recorded on a Varian Saturn 2200 GCMS spectrometer. Quantum mechanical calculations were used to carry out the optimized geometry and TD-DFT

Fig. 1 Absorption spectra of Schiff bases **1–4**
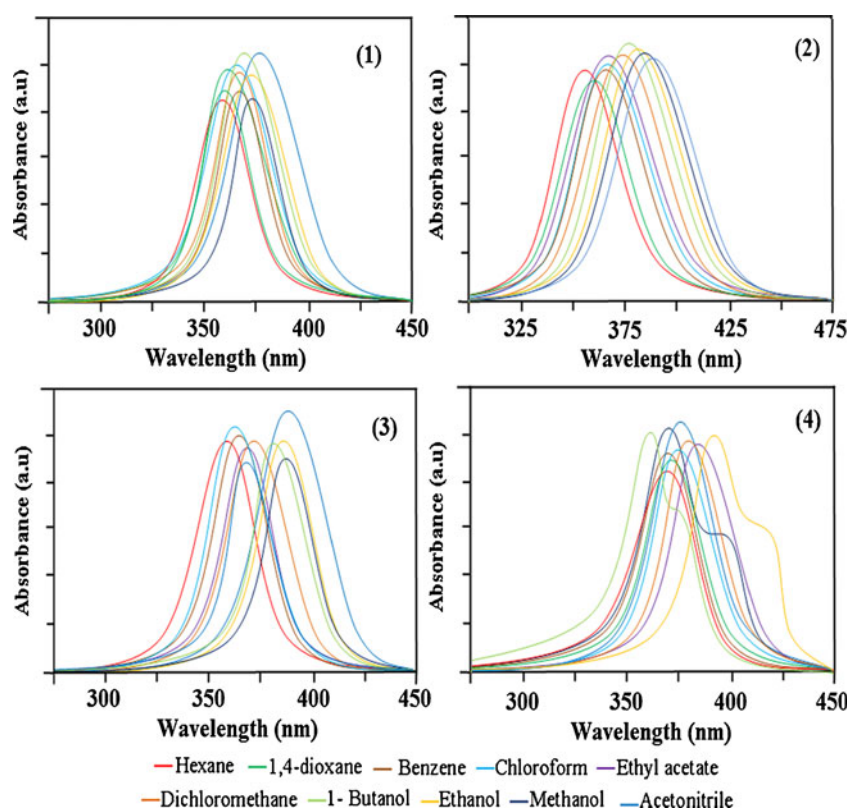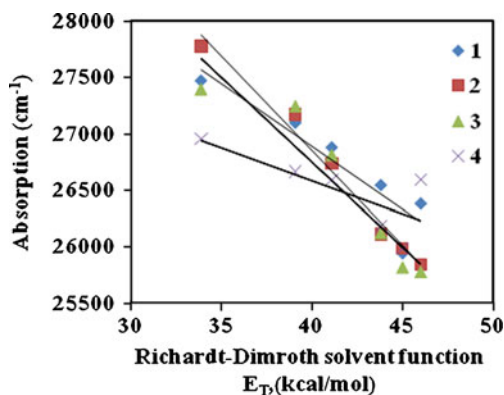
Fig. 2 Correlation of solvent shifts of absorption with Reichardt-Dimroth solvent E_T parameters for **1–4**

with Guassian-03 program using the Becke3-Lee-Yang-Parr (B3LYP) functional supplemented with the standard 6–31 G(d,p) basis set [19].

General Procedure for the Synthesis of Schiff Bases

The Schiff bases (**1–4**) were synthesized according to the procedure reported in literature [20]. A solution of p-aminoazobenzene (1 mmol) and the corresponding heterocyclic aldehydes (1.5 mmol) in 20 ml absolute ethanol was refluxed for 2 h. The resulting precipitate was filtered off and purified by column chromatography.

(0E,4E)-4-(2-Phenyldiazenyl)-N-(2-Thiophenylidene) Benzenamine (**1**)

Yield: 78%, m.p: 142 °C. Anal. calcd. for $C_{17}H_{13}N_3S$: C, 70.08; H, 4.50; N, 14.42. Found: C, 69.76; H, 4.17; N, 13.75. MS: m/z 291.00, calcd. 291.08. 160.24. ^{1}H NMR: 8.66 (s, 1H), 8.01 (d, 2H), 7.96 (d, 2H), 7.86 (m, 1H), 7.49–7.59 (m, 2H), 7.43 (t, 1H), 7.38 (t, 1H), 7.29 (s, 1H), 7.19 (t, 1H), 6.77 (d, 1H). ^{13}C NMR: 153.61, 153.00, 150.79, 149.58, 145.60, 142.66, 132.87, 130.85, 129.81, 129.11, 129.06, 129.01, 128.98, 125.13, 124.10, 122.81, 122.36, 121.77, 114.64.

(0E,4E)-4-(2-Phenyldiazenyl)-N-(2-Furfurylidene) Benzenamine (**2**)

Yield: 78%, m.p: 137 °C. Anal. calcd. for $C_{17}H_{13}N_3O$: C, 74.17; H, 4.76; N, 15.26. Found: C, 73.46; H, 4.43; N, 14.86. MS: m/z 274.00, calcd. 275.11. ^{1}H NMR: 8.44 (s, 1H), 8.10 (s, 1H), 7.84–7.97 (m, 3H), 7.53–7.45 (m, 4H), 7.29 (s, 1H), 6.77 (d, 1H). ^{13}C NMR: 152.76, 129.34, 129.08, 128.97, 125.12, 124.78, 124.75, 124.03, 123.90, 123.79, 122.99, 117.01, 116.96, 116.56, 114.63.

(0E,4E)-4-(2-Phenyldiazenyl)-N-(2-Pyridylidene) Benzenamine (**3**)

Yield: 87%, m.p: 116 °C. Anal. calcd. for $C_{18}H_{14}N_4$: C, 76.17; H, 5.43; N, 13.32. Found: C, 75.50; H, 4.93; N, 19.57. MS: m/z 285.00, calcd. 286.12. ^{1}H NMR: 8.77 (bd, 1H), 8.69 (s, 1H), 8.04 (m, 1H), 7.41–7.45 (m, 3H), 7.49–7.52 (m, 2H), 7.53–7.57 (m, 2H), 7.84–7.88 (m, 3H), 7.96 (m, 1H). ^{13}C NMR: 161.41, 154.35, 153.31, 153.00, 152.75, 149.59, 145.59, 137.07, 136.76, 130.96, 129.86, 129.80, 129.11.

(0E,4E)-4-(2-Phenyldiazenyl)-N-(o-Hydroxypyridylidene) Benzenamine (**4**)

Yield: 83%, m.p: 123 °C. Anal. calcd. for $C_{18}H_{14}N_4O$: C, 70.35; H, 4.67; N, 18.53. Found: C, 70.15; H, 4.23; N, 17.98. MS: m/z 301.00, calcd. 302.12. ^{1}H NMR: 8.51 (s, 1H), 8.01 (s, 1H), 7.45–7.93 (m, 5H), 7.45–7.53 (m, 4H), 7.39 (s, 1H), 6.97 (d, 1H), 4.91 (s, 1H). ^{13}C NMR: 155.67, 152.32, 151.75, 140.12, 139.47, 131.32, 129.46, 127.53, 124.11, 122.79.

Results and Discussion

Photophysical Characterization of (**1–4**)

UV-visible absorption and fluorescence emission spectra of dye derivatives in a series of solvents of varying polarity and their photophysical properties are compiled in Table 1. The main absorption band attributed to the π-π* transition since in aminobenzene dyes, n-π* and π-π* transitions are in close proximity, the low intensity n-π* transition is completely overlaid by the intensive π-π* transition [20, 21]. Theoretical calculations were carried out to study the absorption transition in dichloromethane and the calculated
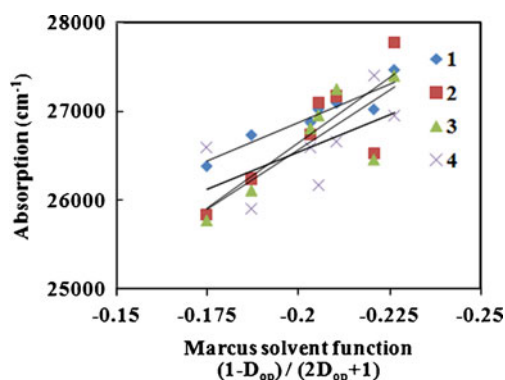
Fig. 3 Correlation of solvent shifts of absorption with Marcus solvent optical dielectric functions for **1–4**

**Fig. 4** Emission spectra of Schiff bases **1**–**4**
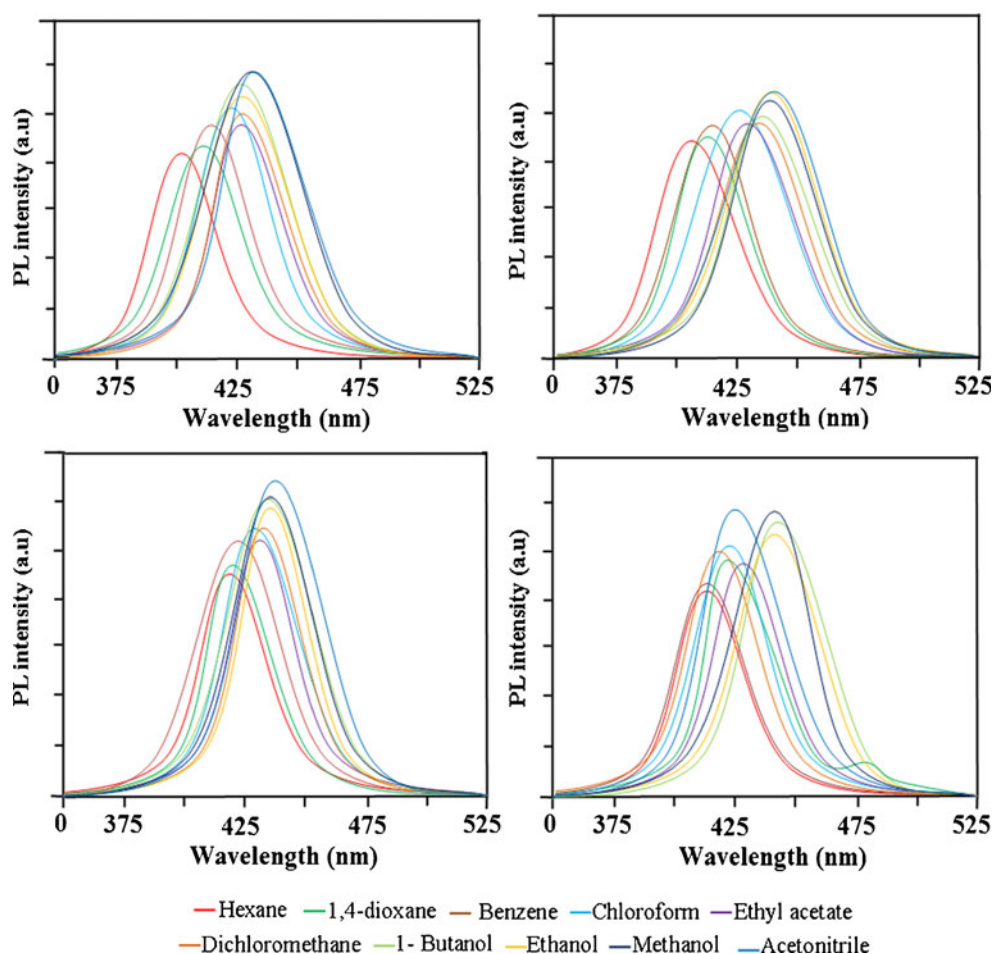
absorption maxima are in good agreement with the experimental absorption maxima.

Measurement of absorption solvatochromism (Fig. 1) have been interpreted with Marcus and Reichardt-Dimroth solvent functions to estimate the transition dipoles associated with low lying excited state. The linear correlation (Fig. 2) of solvent shift of absorption band position of dyes (**1**–**4**) with Reichardt-Dimroth solvent E_T parameters is indicative of the fact that the dielectric solute solvent interactions are responsible for the observed solvatochromic shift for these dye derivatives. The observed linear correlation (Fig. 3) of solvent shift of absorption band positions of **1**–**4** with Marcus optical dielectric solvent function $[(1 - D_{op})/(2D_{op} + 1)]$ reveals that transition dipoles associated with absorption and the direction of excited dipole is opposite to that of the ground state-dipole [22].

Solvatochromism of Dye Derivatives—Lippert-Mataga Plot

All these dye derivatives **1**–**4** show solvatochromism (Fig. 4) i.e., changes in the polarity of the solvents, charge

transfer takes place and causing colour changes. The position of the longer-wavelength absorption and emission bands in the spectra was determined in several protic and aprotic solvents. Lippert-Mataga [23] plot (Fig. 5) was
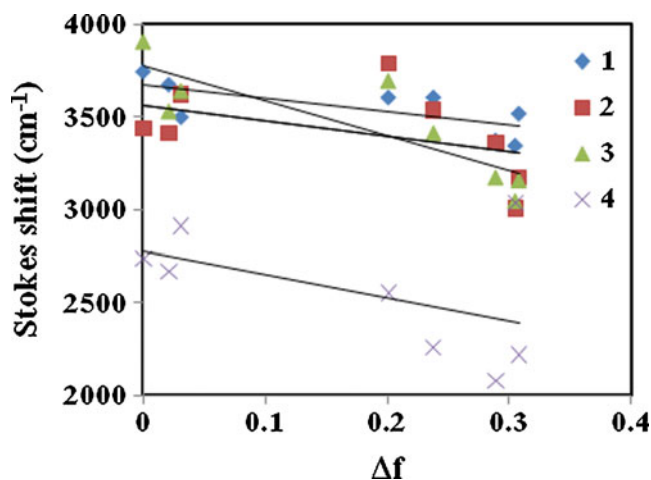
Fig. 5 Lippert-Mataga plot of **1**–**4**

constructed for the normal fluorescence spectra of dye derivatives (**1–4**) using the following equation.

$$\bar{v}_{ss} = \bar{v}_{ab} - \bar{v}_{fl} = const + \left[\frac{2\left(\mu_e - \mu_g\right)^2}{hca^3} \right] f(D, n) \qquad (1)$$

where $f(D, n) = (D - 1)/(2D + 1) - (n^2 - 1)/(2n^2 + 1)$, indicates the orientation polarizability and depicts polarity parameter of the solvent [24], n is refractive index, D is dielectric constant, μ_e and μ_g are dipole moments of the species in S_1 and S_0 states, respectively, h, Planck's constant; c, velocity of light and a, Onsager's cavity radius. The Lippert-Mataga plot is linear for the non-polar and polar/

aprotic solvents with excellent correlation coefficient. Large stokes shifted fluorescence band suggests that this emission has originated from the species which is not present in the S_0 state and large geometrical changes have takes place in the species when excited to S_1 state.

The higher bathochromic shifts observed in the fluorescence band of the dye derivatives can be interpreted by the Brunings-Corwin effect [25]. Because the distortion of the geometry in the excited state, the fluorescence band is bathochromically shifted to a higher extent than the absorption band. Moreover, the loss of planarity in the excited state of the dye derivatives explained the lower fluorescence quantum yield in apolar solvents owing to an increase in the non-radiative processes [26, 27].

Table 2 Adjusted Coefficients ($(\upsilon_x)_0$, c_a, c_b and c_c) and Correlation Coefficients (r) for the Multilinear Regression Analysis of the Absorption υ_{ab} and Fluorescence υ_{fl} Wavenumbers and Stokes Shift ($\Delta\upsilon_{ss}$) of Schiff base derivatives **1–4** with the Solvent Polarity/Polarizability, and the Acid and Base Capacity Using the Taft (π^*, α and β) and the Catalan (SPP^N, SA and SB) Scales

1	Kamlet-Taft	$(\upsilon_x)_0\,cm^{-1}$	(π^*)	c_α	c_β	r
	λ_{ab}	$(2.74\pm0.02)\times10^4$	$(9.44\pm3.17)\times10^3$	$(16.27\pm96.22)\times10^3$	$-(7.71\pm7.27)\times10^3$	0.93
	λ_{fl}	$(2.36\pm0.01)\times10^4$	$(5.48\pm2.31)\times10^3$	$(10.08\pm7.02)\times10^3$	$-(5.27\pm5.306)\times10^3$	0.88
	$\Delta\upsilon_{ss}=\upsilon_{ab}-\upsilon_{fl}$	$(0.37\pm0.01)\times10^4$	$-(3.96\pm2.02)\times10^3$	$(6.14\pm6.15)\times10^3$	$-(2.44\pm4.651)\times10^3$	0.86
	Catalan	$(\upsilon_x)_0\,cm^{-1}$	c_{SPP}^N	c_{SA}	c_{SB}	r
	λ_{ab}	$(2.73\pm0.03)\times10^4$	$(14.96\pm11.18)\times10^3$	$(51.79\pm47.14)\times10^3$	$-(50.20\pm48.95)\times10^3$	0.53
	λ_{fl}	$(2.36\pm0.02)\times10^4$	$(12.65\pm6.01)\times10^3$	$(46.62\pm25.35)\times10^3$	$-(45.63\pm26.32)\times10^3$	0.61
	$\Delta\upsilon_{ss}=\upsilon_{ab}-\upsilon_{fl}$	$(0.37\pm0.01)\times10^4$	$-(2.31\pm5.83)\times10^3$	$(5.72\pm24.59)\times10^3$	$-(4.57\pm25.54)\times10^3$	0.40
2	Kamlet-Taft	$(\upsilon_x)_0\,cm^{-1}$	(π^*)	c_α	c_β	r
	λ_{ab}	$(2.73\pm0.01)\times10^4$	$(5.49\pm2.69)\times10^3$	$(9.86\pm8.18)\times10^3$	$-(4.56\pm6.19)\times10^3$	0.82
	λ_{fl}	$(2.42\pm0.01)\times10^4$	$(7.09\pm5.66)\times10^3$	$(12.70\pm17.20)\times10^3$	$-(6.42\pm13.00)\times10^3$	0.68
	$\Delta\upsilon_{ss}=\upsilon_{ab}-\upsilon_{fl}$	$(0.31\pm0.)\times10^4$	$-(15.92\pm3.36)\times10^3$	$-(2.84\pm10.22)\times10^3$	$(1.86\pm7.73)\times10^3$	0.48
	Catalan	$(\upsilon_x)_0\,cm^{-1}$	c_{SPP}^N	c_{SA}	c_{SB}	r
	λ_{ab}	$(2.74\pm0.01)\times10^4$	$(6.07\pm2.75)\times10^3$	$(10.86\pm8.25)\times10^3$	$-(5.11\pm6.21)\times10^3$	0.88
	λ_{fl}	$(2.45\pm0.02)\times10^4$	$(8.73\pm4.42)\times10^3$	$(15.57\pm13.24)\times10^3$	$-(7.97\pm9.77)\times10^3$	0.88
	$\Delta\upsilon_{ss}=\upsilon_{ab}-\upsilon_{fl}$	$(0.29\pm0.013)\times10^4$	$-(2.66\pm2.19)\times10^3$	$-(4.70\pm6.57)\times10^3$	$(2.87\pm4.95)\times10^3$	0.85
3	Kamlet-Taft	$(\upsilon_x)_0\,cm^{-1}$	(π^*)	c_α	c_β	r
	λ_{ab}	$(2.73\pm0.04)\times10^4$	$(0.47\pm6.99)\times10^3$	$-(3.46\pm22.77)\times10^3$	$-(3.20\pm17.76)\times10^3$	0.31
	λ_{fl}	$(2.38\pm0.03)\times10^4$	$(0.054\pm5.91)\times10^3$	$(3.37\pm19.25)\times10^3$	$-(2.71\pm15.01)\times10^3$	0.32
	$\Delta\upsilon_{ss}=\upsilon_{ab}-\upsilon_{fl}$	$(0.35\pm0.01)\times10^4$	$-(0.04\pm2.75)\times10^3$	$(0.075\pm8.96)\times10^3$	$-(0.50\pm6.99)\times10^3$	0.61
	Catalan	$(\upsilon_x)_0\,cm^{-1}$	c_{SPP}^N	c_{SA}	c_{SB}	r
	λ_{ab}	$(2.75\pm0.03)\times10^4$	$(22.22\pm11.18)\times10^3$	$(81.54\pm47.13)\times10^3$	$-(80.21\pm48.94)\times10^3$	0.61
	λ_{fl}	$(2.40\pm0.02)\times10^4$	$(20.92\pm9.32)\times10^3$	$(76.11\pm39.26)\times10^3$	$-(73.14\pm40.77)\times10^3$	0.62
	$\Delta\upsilon_{ss}=\upsilon_{ab}-\upsilon_{fl}$	$(0.35\pm0.01)\times10^4$	$-(1.30\pm5.42)\times10^3$	$(5.43\pm22.82)\times10^3$	$-(7.07\pm23.70)\times10^3$	0.61
4	Kamlet-Taft	$(\upsilon_x)_0\,cm^{-1}$	(π^*)	c_α	c_β	r
	λ_{ab}	$(2.68\pm0.03)\times10^4$	$(13.64\pm2.61)\times10^3$	$-(55.69\pm8.51)\times10^3$	$(46.91\pm6.64)\times10^3$	0.92
	λ_{fl}	$(2.41\pm0.01)\times10^4$	$(0.31\pm1.30)\times10^3$	$-(7.24\pm4.24)\times10^3$	$(5.71\pm3.31)\times10^3$	0.97
	$\Delta\upsilon_{ss}=\upsilon_{ab}-\upsilon_{fl}$	$(0.26\pm0.01)\times10^4$	$-(13.33\pm1.98)\times10^3$	$-(48.45\pm6.44)\times10^3$	$-(41.20\pm5.02)\times10^3$	0.95
	Catalan	$(\upsilon_x)_0\,cm^{-1}$	c_{SPP}^N	c_{SA}	c_{SB}	r
	λ_{ab}	$(2.66\pm0.03)\times10^4$	$(6.98\pm13.46)\times10^3$	$-(23.72\pm56.73)\times10^3$	$(12.81\pm58.92)\times10^3$	0.62
	λ_{fl}	$(2.39\pm0.02)\times10^4$	$(0.70\pm6.96)\times10^3$	$-(20.32\pm29.34)\times10^3$	$(26.66\pm30.47)\times10^3$	0.80
	$\Delta\upsilon_{ss}=\upsilon_{ab}-\upsilon_{fl}$	$(0.27\pm0.04)\times10^4$	$-(6.28\pm14.38)\times10^3$	$-(3.39\pm60.62)\times10^3$	$-(13.85\pm62.95)\times10^3$	0.45

Fig. 6 a Stabilizing interaction of **1–3** with basic solvents. **b** ESIPT process in Schiffs base **4**
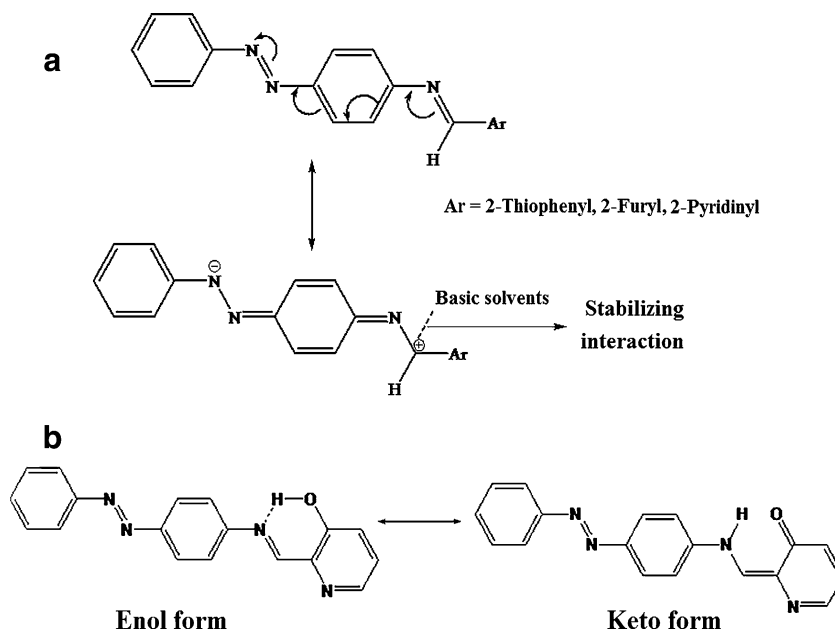
The solvent effect on ν_{abs}, ν_{em}, and $\Delta\nu_{ss}$ can also be described on the basis of a multi-linear expression (Eq. 2):

$$y = y_0 + aA + bB + cC \qquad (2)$$

in which y_0 stands for the physicochemical property of interest in the absence of solvent (i.e., in the gas phase); a, b, and c are adjustable coefficients that reflect the dependency of the physicochemical property (y) in a given solvent on the various (A, B, C) solvent parameters. At least two different sets of solvent scales can be found in the literature to characterize these solvent properties. In the present analysis, the polarity/polarizability, the acidity and the basicity of the solvent are considered. Kamlet and Taft [28] put forward the π^*, α and β parameters to character-

Fig. 7 a Correlation between the experimental absorption wavenumber with the predicted values obtained by a multicomponent linear regression using the π^*, α and β-scale (Taft) solvent parameters for **1–4**. **b** Correlation between the experimental fluorescence wavenumber with the predicted values obtained by a multicomponent linear regression using the π^*, α and β-scale (Taft) solvent parameters for **1–4**
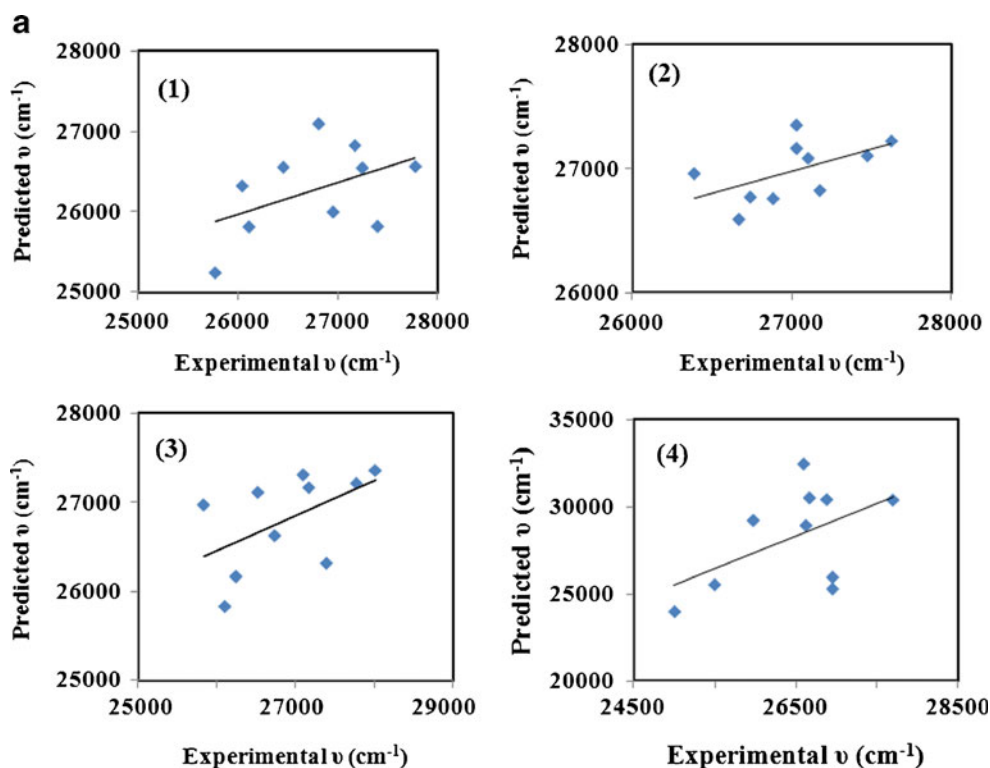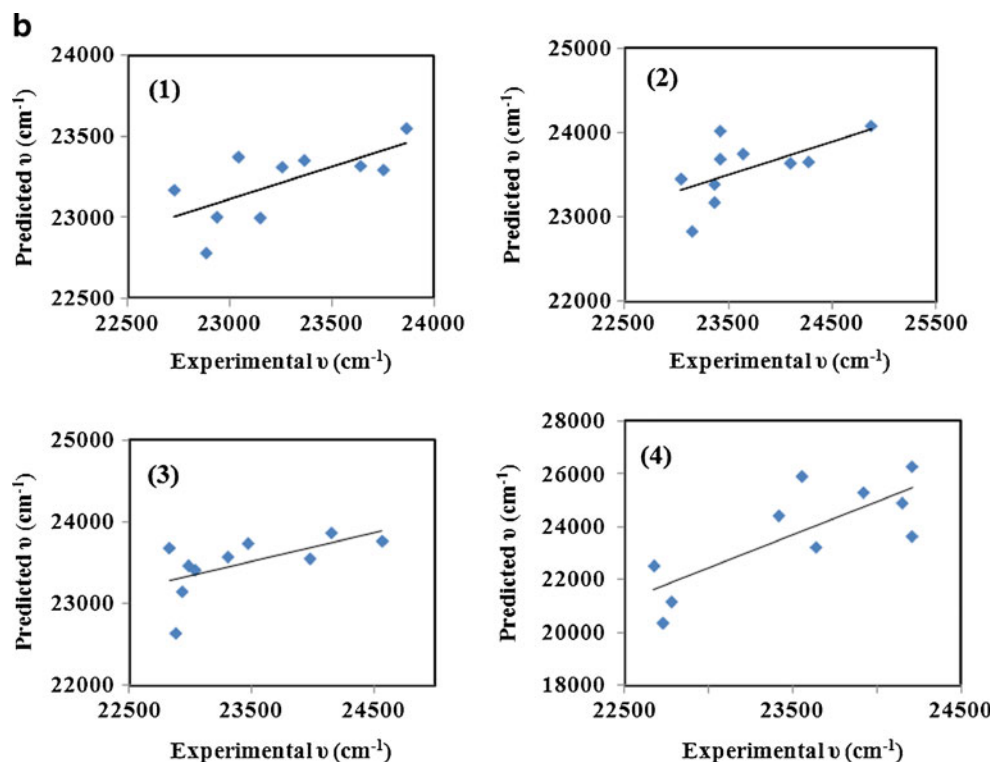
Fig. 7 (continued)

ize, respectively, the polarity/polarizability, the acidity, and the basicity of a solvent (Eq. 2). Conversely, Catalan et al. proposed an empirical solvent scales for polarity/polarizability [29–32] (SPP), acidity [30] (SA) and basicity [30, 31] (SB) to describe the respective properties of a given solvent (Eq. 3).

$$y = y_0 + a_\alpha \alpha + b_\beta \beta + c_{\pi*} \pi* \qquad (Kamlet - Taft) \qquad (2)$$

$$y = y_0 + a_{SA} SA + b_{SB} SB + c_{SPP} SPP \qquad (Catalan) \qquad (3)$$

The dominant coefficient affecting the absorption and fluorescence band of dye derivatives **1**–**4** is the polarity/polarizability of the solvent [$C_{\pi*}$ or $C_{SPP}{}^N$] having a positive value, corroborating the solvatochromic shifts with the solvent polarity. For **1**–**3**, the adjusted coefficient representing the electron releasing ability or basicity of the solvent, C_β or C_{SB} has the large negative values (Table 2), suggesting solvent basicity play an important role in absorption and fluorescence displacements which can be due to the existence of positive charge on the imine carbon so that the basic solvent stabilize the
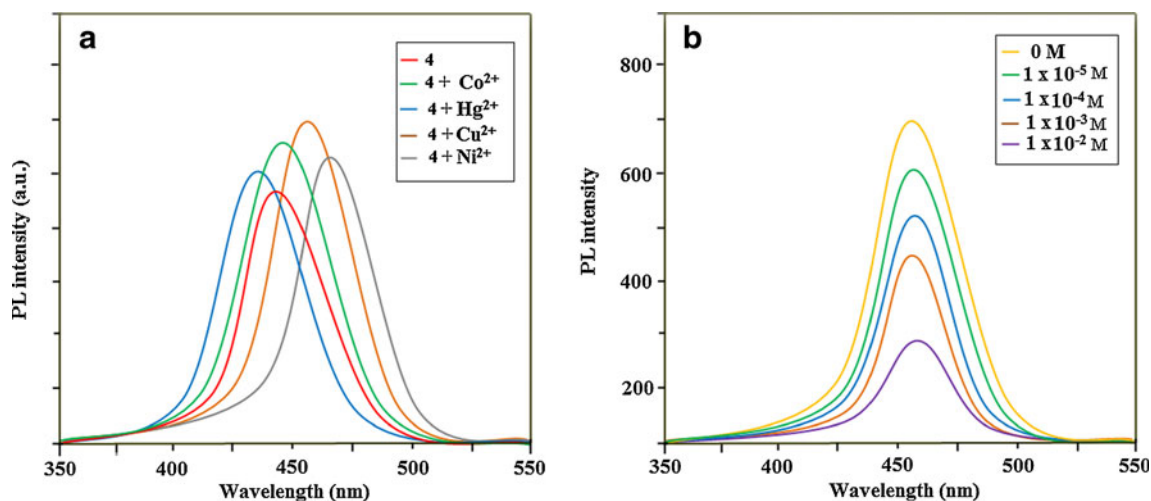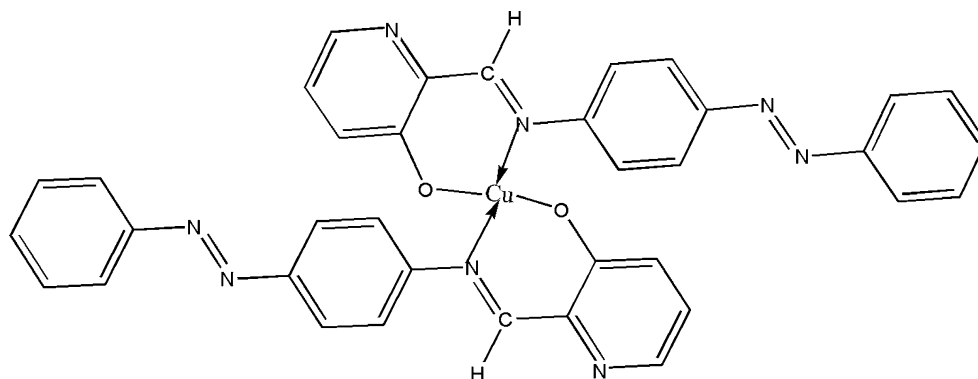

Fig. 8 (a) Fluorescence spectra of Schiffs base (4) in the presence of various metal ions. b Fluorescence chemisensors blocking by metal ion binding

Fig. 9 Possible structure of Schiffs base (**4**)-Cu^{2+} complex

structures and cause solvatochromic shifts (Fig. 6a). In the case of **4,** the coefficient controlling the H-donor capacity or acidity of the solvent, C_α or C_{SA}, has the negative values (Table 2), suggesting that the absorption and fluorescence bands shifted to lower energies with the increasing acidity of the solvent. This effect can be due to the existence of keto-enol tautomers of **4** due to ESIPT process (Fig. 6b). The existence of good correlations (Fig. 7a and b) between the absorption and fluorescence wavenumbers calculated by the multicomponent linear regression employing the Taft-proposed solvent parameters and the obtained correlation coefficients are tabulated in Table 2. The two sets of solvent parameters gives qualitatively similar results.

The changes in the fluorescence properties of **4** caused by different metal ions such as Co^{2+}, Hg^{2+}, Ni^{2+} and Cu^{2+} were measured in ethanol. The fluorescence of **4** quenched markedly with the gradual addition of Cu^{2+} (Fig. 8). The quenching in fluorescence intensity of Schiff base by the addition of Cu^{2+} cation indicates the complexation of Schiff base with Cu^{2+}, the Schiff base has bidentate sites and forming the expected Cu^{2+} complex (Fig. 9). The possible reason for the fluorescence quenching is the formation of a ground state non-fluorescent complex **4**-Cu^{2+}. According to the obtained results, Schiff base (**4**) can be used as a new fluorescence sensor to detect the quantity of Cu^{2+} ion in any sample solution depending on the relative intensity change.

Conclusion

The present study reports the solvatochromic effect on the fluorometric behaviour of Schiff base derivative in different solvents with varying polarity. The fluorescence property of the molecule is very much sensitive to the polarity and the protic character of the solvent. The presence of distortion from planarity in the Schiff base in the excited state leads to solvatochromic shifts.

We have developed a new fluorescent chemisensor for transition metal ions Hg^{2+}, Pb^{2+} and Cu^{2+} ions Co^{2+}.

References

1. Nejati K, Rezvani Z, Massoumi B (2007) Syntheses and investigation of thermal properties of copper complexes with azo-containing Schiff-base dyes. Dye Pigment 75:653–657
2. Peker E, Serin S (2004) Synthesis and characterization of some cobalt(II), copper(II), and nickel(II) complexes with new schiff bases from the reaction of p-aminoazobenzene with salicylaldehydes. 34: 859–872
3. Souza P, Garcia-Vázquez JA, Masaguer JR (1985) Synthesis and characterization of copper(II) and nickel(II) complexes of the Schiff base derived from 2-(2-aminophenyl)benzimidazole and salicylaldehydes. 10: 410–412
4. Naeimi H, Safari J, Heidarnezhad A (2007) Synthesis of Schiff base ligands derived from condensation of salicylaldehyde derivatives and synthetic diamines. 73: 251–253
5. Lippard SJ, Berg JM (1994) Principles of bioinorganic chemistry. University Science, California
6. Wang YW, Shi YT, Peng Y, Zhang AJ, Ma TH, Dou W, Zheng JR (2009) Fluorescent sensors for Ca(2+) and Pb(2+) based on binaphthyl derivatives. Spectrochim Acta A 72:322–326
7. Singh N, Kaur N, Dunn J, MacKay M, Callan JF (2009) A new fluorescent chemosensor for iron(III) based on the β-aminobisulfonate receptor. Tetrahedron Lett 50:953–956
8. Oter O, Ertekin K, Kilincarslan R, Ulusoy M, Cetinkaya B (2007) Photocharacterization of a novel fluorescent Schiff base and investigation of its utility as an optical Fe^{3+} sensor in PVC matrix. Dye Pigment 74:730–735
9. Guo L, Hong S, Lin X, Xie Z, Chen G (2008) An organically modified sol–gel membrane for detection of lead ion by using 2-hydroxy-1-naphthaldehydene-8-aminoquinoline as fluorescence probe. Sensor Actuator B 130:789–794
10. Farrugia G, Lotti S, Prodi L, Zaccheroni N, Montalti M, Savage PB, Andreani G, Trapani V, Wolf FI (2009) A simple spectrofluorometric assay to measure total intracellular magnesium by a hydroxyquinoline derivative. J Fluoresc 19:11–19

11. Shah M, Thangaraj K, Soong ML, Wolford LT, Boyer JH, Politzer IR, Pavlopoulos TG (1990) Pyrromethene-BF2 complexes as laser dyes: 1. Heteroat Chem 1:389–399

12. Pavlopoulos TG, Boyer JH, Thangaraj K, Sathyamoorthi G, Soong ML (1992) Laser dye spectroscopy of some pyrromethene-BF$_2$ complexes. Appl Opt 31:7089–7094

13. Lopez Arbeloa F, Ruiz Ojeda P, Lopez Arbeloa I (1988) On the aggregation of rhodamine B in ethanol. Chem Phys Lett 148:253–258

14. Costela A, Moreno IG, Sastre R (2001) In: Nalwa HS (ed) Handbook of advanced electronic and photonic materials and devices. Academic, San Diego, pp 7–161

15. O'Neil MP (1993) Synchronously pumped visible laser dye with twice the efficiency of rhodamine 6G. Opt Lett 18:37–38

16. Rhan MD, King TA (1995) Comparison of laser performance of dye molecules in sol-gel, polycom, ormosil, and poly(methyl methacrylate) host media. Appl Opt 34:8260–8271

17. Yariv E, Schultheiss S, Saraidarov T, Reisfeld R (2001) Efficiency and photostability of dye doped solid state lasers in different hosts. Opt Mater 16:29–38

18. Lopez Arbeloa F, Lopez Arbeloa I, Lopez Arbeloa T (2001) In: Nalwa HS (ed) Handbook of advanced electronic and photonic materials and devices. Academic, San Diego, pp 7–209

19. Gaussian 03 program, (Gaussian Inc., Wallingford CT) 2004

20. Jayabharathi J, Thanikachalam V, Srinivasan N, Venkatesh Perumal M, Jayamoorthy K (2011) A physiochemical study of excited state intramolecular proton transfer process Luminescent chemosensor by spectroscopic investigation supported by abinitio calculations. Spectrochim Acta A 79:137–147

21. Gabor G, Frei YF, Fischer E (1968) Tautomerism and geometric isomerism in arylazophenols and naphthols. IV. Spectra and reversible photoreactions of m- and p-hydroxyazobenzene. J Phys Chem 72:3266–3272

22. Wilde AP, Watts RJ (1991) Solvent effects on metal-to-ligand charge-transfer bands in ortho-metalated complexes of iridium (III): estimates of transition dipole moments. J Phys Chem 95:622–629

23. Balamurali MM, Dogra SK (2004) Intra- and intermolecular proton transfer in methyl-2-hydroxynicotinate. J Luminesc 110:147–163

24. Mazumdar S, Manoharan R, Dogra SK (1989) Solvatochromic effects in the fluorescence of a few diamino aromatic compounds. J Photochem Photobiol A 46:301–314

25. Hofer JE, Grabenstetter RJ, Wiig EO (1950) The fluorescence of cyanine and related dyes in the monomeric state. J Am Chem Soc 72:203–209

26. Assor Y, Burshtein Z, Rosenwaks S (1998) Spectroscopy and laser characteristics of copper-vapor-laser pumped pyrromethene-556 and pyrromethene-567 dye solutions. Appl Opt 37:4914–4920

27. Lopez Arbeloa I (1980) Fluorescence quantum yield evaluation. reabsorption and reemission corrections. J Photochem 14:97–105

28. Kamlet MJ, Taft RW (1976) The solvatochromic comparison method. I. The β-scale of solvent Hydrogen-Bond Acceptor (HBA) basicities. J Am Chem Soc 98:377–383

29. Catalan J (1997) On the E$_T$(30), α^*, Py, S , and SPP empirical scales as descriptors of nonspecific solvent effects. J Org Chem 62:8231–8234

30. Catalan J, Diaz CA (1997) A generalized solvent acidity scale: the solvatochromism of o-tert-butylstilbazolium betaine dye and its homomorph o, o′-di-tert-butylstilbazolium betaine dye. Liebigs Ann 1997:1941–1949

31. Catalan J, Palomar J, Diaz C, de Paz JLG (1997) On solvent basicity: analysis of the SB scale. J Phys Chem A 101:5183–1589

32. Catalan J (2001) In: Wypych G (ed) Handbook of solvents. ChemTec Publishing, Toronto, pp 583–616